
AFRL-RZ-WP-TP-2010-2090

# FINITE-ELEMENT SIMULATIONS OF FIELD AND CURRENT DISTRIBUTIONS IN MULTIFILAMENTARY SUPERCONDUCTING FILMS (POSTPRINT)

**Timothy J. Haugan and Paul N. Barnes**

**Mechanical Energy Conversion Branch**
**Energy/Power/Thermal Division**

**Andrea Lucarelli**

**Laboratorium für Festkörperphysik**

**Francesco Grilli**

**Ecole Polytechnique Montréal**

**Gunter Lüpke**

**The College of William and Mary**

**MARCH 2010**



**AIR FORCE RESEARCH LABORATORY**
**PROPULSION DIRECTORATE**
**WRIGHT-PATTERSON AIR FORCE BASE, OH 45433-7251**
**AIR FORCE MATERIEL COMMAND**
**UNITED STATES AIR FORCE**

# REPORT DOCUMENTATION PAGE

*Form Approved*
*OMB No. 0704-0188*



| 1. REPORT DATE *(DD-MM-YY)* | 2. REPORT TYPE | 3. DATES COVERED *(From - To)* |
|---|---|---|
| March 2010 | Journal Article Postprint | 21 September 2007 – 21 September 2009 |

**4. TITLE AND SUBTITLE**

FINITE-ELEMENT SIMULATIONS OF FIELD AND CURRENT DISTRIBUTIONS IN MULTIFILAMENTARY SUPERCONDUCTING FILMS (POSTPRINT)

**5a. CONTRACT NUMBER**
In-house

**5b. GRANT NUMBER**

**5c. PROGRAM ELEMENT NUMBER**
62203F

**6. AUTHOR(S)**

Timothy J. Haugan and Paul N. Barnes (AFRL/RZPG)
Andrea Lucarelli (Laboratorium für Festkörperphysik)
Francesco Grilli (Ecole Polytechnique Montréal)
Gunter Lüpke (The College of William and Mary)

**5d. PROJECT NUMBER**
3145

**5e. TASK NUMBER**
32

**5f. WORK UNIT NUMBER**
314532ZE

**7. PERFORMING ORGANIZATION NAME(S) AND ADDRESS(ES)**

Mechanical Energy Conversion Branch (AFRL/RZPG)
Energy/Power/Thermal Division
Air Force Research Laboratory, Propulsion Directorate
Wright-Patterson Air Force Base, OH 45433-7251
Air Force Materiel Command, United States Air Force

---

Laboratorium für Festkörperphysik
CH-8093
Zürich, Switzerland

Ecole Polytechnique Montréal
Montréal, Canada

---

The College of William and Mary
Department of Applied Science
Williamsburg, VA 23187-8795

**8. PERFORMING ORGANIZATION REPORT NUMBER**
AFRL-RZ-WP-TP-2010-2090

**9. SPONSORING/MONITORING AGENCY NAME(S) AND ADDRESS(ES)**

Air Force Research Laboratory
Propulsion Directorate
Wright-Patterson Air Force Base, OH 45433-7251
Air Force Materiel Command
United States Air Force

**10. SPONSORING/MONITORING AGENCY ACRONYM(S)**
AFRL/RZPG

**11. SPONSORING/MONITORING AGENCY REPORT NUMBER(S)**
AFRL-RZ-WP-TP-2010-2090

**12. DISTRIBUTION/AVAILABILITY STATEMENT**

Approved for public release; distribution unlimited.

**13. SUPPLEMENTARY NOTES**

Journal article published in the *Superconductor Science and Technology*, Vol. 22 (2009).
PA Case Number: 88ABW-2008-1037; Clearance Date: 18 Nov 2008.



**14. ABSTRACT**

We present a finite-element model for computing current and field distributions in multifilamentary superconducting thin films subjected to simultaneous effects of a transport ac current and a perpendicularly applied dc field. The model is implemented in the finite-element software package COMSOL Multiphysics and this solves Maxwell equations using a highly nonlinear resistivity to describe electrical superconducting characteristics. The time-dependent magnetic flux, current distributions, and ac losses are studied for different distances between filaments. We find that increasing the interfilamentary distance affects the transport and screening current distributions, reducing both the magnetic coupling and ac losses.

**15. SUBJECT TERMS**

superconductivity, flux pinning, critical current density, magnetic field, $YBa_2Cu_3O_{7-z}$ or YBCO, finite-element model simulation, COMSOL, multiphysics, maxwell equations, magnetic flux, current distributions, ac loss, multifilament wires, screening current distributions, magnetic coupling

| 16. SECURITY CLASSIFICATION OF: | | | 17. LIMITATION OF ABSTRACT: | 18. NUMBER OF PAGES | 19a. NAME OF RESPONSIBLE PERSON (Monitor) |
|---|---|---|---|---|---|
| a. REPORT | b. ABSTRACT | c. THIS PAGE | | | Timothy J. Haugan |
| Unclassified | Unclassified | Unclassified | SAR | 12 | 19b. TELEPHONE NUMBER *(Include Area Code)* N/A |

**Standard Form 298 (Rev. 8-98)**
Prescribed by ANSI Std. Z39-18

Supercond. Sci. Technol. **22** (2009) 105015 (6pp) doi:10.1088/0953-2048/22/10/105015

# Finite-element simulations of field and current distributions in multifilamentary superconducting films

**Andrea Lucarelli[1,2], Francesco Grilli[3,4], Gunter Lüpke[2], Timothy J Haugan[5] and Paul N Barnes[5]**

[1] Laboratorium für Festkörperphysik, ETH-Zürich, CH-8093 Zürich, Switzerland
[2] Department of Applied Science, The College of William and Mary, Williamsburg, VA 23187-8795, USA
[3] Ecole Polytechnique Montréal, Montréal, Canada
[4] Institute for Technical Physics, Forschungszentrum Karlsruhe, D-76344 Eggenstein-Leopoldshafen, Germany
[5] Air Force Research Laboratory, Wright-Patterson AFB, OH 45433-7919, USA

Received 24 April 2009, in final form 16 July 2009
Published 21 September 2009
Online at stacks.iop.org/SUST/22/105015

**Abstract**
We present a finite-element model for computing current and field distributions in multifilamentary superconducting thin films subjected to simultaneous effects of a transport ac current and a perpendicularly applied dc field. The model is implemented in the finite-element software package COMSOL Multiphysics and this solves Maxwell equations using a highly nonlinear resistivity to describe electrical superconducting characteristics. The time-dependent magnetic flux, current distributions, and ac losses are studied for different distances between filaments. We find that increasing the interfilamentary distance affects the transport and screening current distributions, reducing both the magnetic coupling and ac losses.

(Some figures in this article are in colour only in the electronic version)

## 1. Introduction

The separation of high-temperature superconducting (HTS) tapes in filaments is a viable approach to reduce ac losses in HTS high power applications, where ac currents and/or ac fields may be applied in addition to any dc field present [1]. Methods such as mechanical [2], laser scribing [3, 4], photolithography [5], or direct printing on buffered substrates using inkjet deposition [6] have been used to create the filaments in the second generation HTS coated conductors in order to reduce hysteretic losses. However, losses of the finely striated tapes can still be noticeably larger than predicted by analytical expressions [7], e.g. due to the addition of coupling currents or lack of field penetration, and such deviation tends to increase with increasing filament density [8]. The magnetic field penetration inside the superconducting filaments is influenced by the field concentration in the non-superconducting interfilamentary trenches or barriers and this magnetic coupling may ultimately affect the losses that depend on the interfilamentary distance [7]. In order to reduce the magnetic coupling between filaments and the associated ac losses, an in-depth understanding of flux and current dynamics in the multifilamentary HTS in realistic conditions is required. This is a complex nonlinear problem that necessitates a multiphysics approach since current and field distributions in superconductors depend strongly on the temperature and history of the applied field and transport current.

In this paper, we report on the effects of different multifilamentary geometries on the current and field dynamics in an ac regime. We used a model for computing the current and field distributions in multifilamentary superconducting thin films subjected to the simultaneous effects of a transport ac current and a perpendicularly applied dc field. In the finite-element simulations, the geometry and the value of the parameters were chosen to allow a direct comparison of the calculated magnetic flux and the current profiles with experimental data obtained by time-resolved magneto-optical imaging (TRMOI) [8], scanning Hall probe [9] and Hall probe arrays [10]. A comparison would provide both a test for the model itself as well as new information on the

 

complex behavior of these systems, as we demonstrated in previous TRMOI studies on HTS single bridged thin films [11]. We find that increasing the interfilamentary distance reduces the magnetic coupling between filaments. The screening and transport currents redistribute more evenly between all filaments. A reduction of magnetic coupling also affects field and current dynamics and decreases the overall ac loss.

## 2. Model description

In this work we neglect the thermal aspects and focus on the electromagnetic characteristics. This means that the superconductor is considered to be at a constant operating temperature below the critical temperature and no quenching occurs. In addition, since the samples are long and straight, a 2D model considering only the superconducting cross-section is utilized.

The electromagnetic fields are described by Faraday's law:

$$\nabla \times \vec{E} = -\frac{\partial \vec{B}}{\partial t}. \tag{1}$$

The superconducting behavior enters the equation by means of a nonlinear relationship between the electric field $E$ and the current density $J$ that gives the electrical resistivity $\rho$:

$$\rho(J) = \frac{E_c}{J_c}\left|\frac{J}{J_c}\right|^{n-1}. \tag{2}$$

The power index $n$ describes the steepness of the transition from superconducting to normal state and is usually put in the perspective of flux flow and flux creep [12]. In the simulation we express the $B$–$H$ relation by using $B = \mu_0 H$, since we are interested in reproducing the flux dynamics of high-temperature and type-II superconductors [13].

The model is implemented in COMSOL Multiphysics [14] general PDE module and uses two magnetic field components as state variables. The use of edge elements of first order allows having the zero-divergence equation for the magnetic field automatically satisfied. Details about the model implementation can be found in [15].

## 3. Simulated problem

In the simulations we consider a system consisting of the air domain and six superconducting filaments 120 $\mu$m wide and 300 nm thick connected at the ends. The dimensions chosen for the system correspond to $YBa_2Cu_3O_{7-x}$ (YBCO) thin films grown by pulsed laser deposition on a $LaAlO_3$ or $SrTiO_3$ substrate and patterned by photolithography to obtain a multifilamentary structure (figure 1). Since the substrate has very poor conductivity and is non-magnetic, it has been neglected in the simulated geometry. These films have been previously studied by TRMOI under the same experimental conditions used in the simulations [16]. The applied field intensity is 5 mT and the ac current $I(t) = I_0 \sin(2\pi f t)$ has an amplitude $I_0 = 8$ A and a frequency $f = 1000$ Hz. For the superconducting material, we choose $J_c = 3 \times 10^{11}$ A m$^{-2}$, $E_c = 10^{-4}$ V m$^{-1}$ and $n = 25$

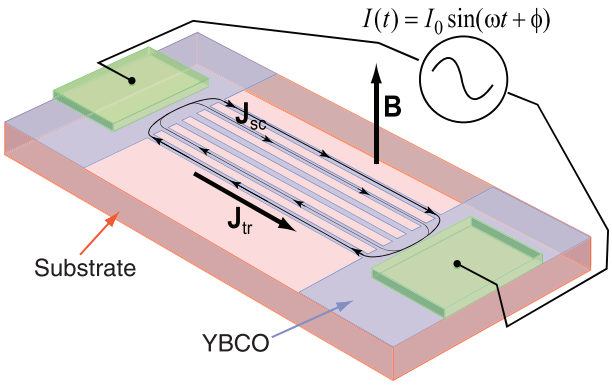


**Figure 1.** Example of filamentary YBCO thin film grown on an insulating substrate with metal contact pads. The dc field B is applied perpendicularly to the film. The screening current $J_{sc}$ flows circularly in the sample, while the ac transport current $J_{tr}$ flows along the filaments.

which are typical values for YBCO films at about 30 K. In order to study effects of geometry on current and field distributions the width of the filaments is fixed at 120 $\mu$m while the distance is varied from 15 to 90 $\mu$m. We simulated three different geometries with width/distance ratios 8/1, 4/1 and 2/1, comparable to multifilamentary coated conductors reported in the literature [2–8].

The model is not restricted to any number of filaments, dimensions or aspect ratios. However, a high aspect ratio of the thin film geometry introduces a large number of nodes that can severely affect the computation time especially for systems with a large number of filaments.

The simulation of two cycles takes about 3–4 h on a workstation equipped with a 2.4 GHz processor and 3 Gb of RAM. In order to avoid transient effects, three complete cycles of the current in 50 steps are simulated.

A circular outer boundary for the air domain is used to impose Dirichlet boundary conditions. An example of the simulated geometry and corresponding mesh is illustrated in figure 2(a). The density of nodes in the mesh increases near the filaments as shown in the detailed view of figure 2(b).

In order to allow direct comparison between simulations and measurements of the field dynamics (e.g. by Hall probe scanning and arrays, SQUID, TRMOI, etc), we calculate magnetic profiles at a height of 1 $\mu$m over the sample surface (see figure 2(b)). This approach has two implications. First, it reduces slightly the intensity of the simulated field profiles, with respect to the profile taken directly in the superconductor, similarly to what happens in the actual measurements, and second, it roughens the profiles adding noise due to the coarsening of the mesh. The latter effect could be avoided refining the mesh in that region but at the cost of an increased calculation time.

## 4. Field dynamics

In figure 3 we present field profiles at different phase points for three different geometries adopted in the simulations. We also plot magnetic flux distributions as time-dependent field maps

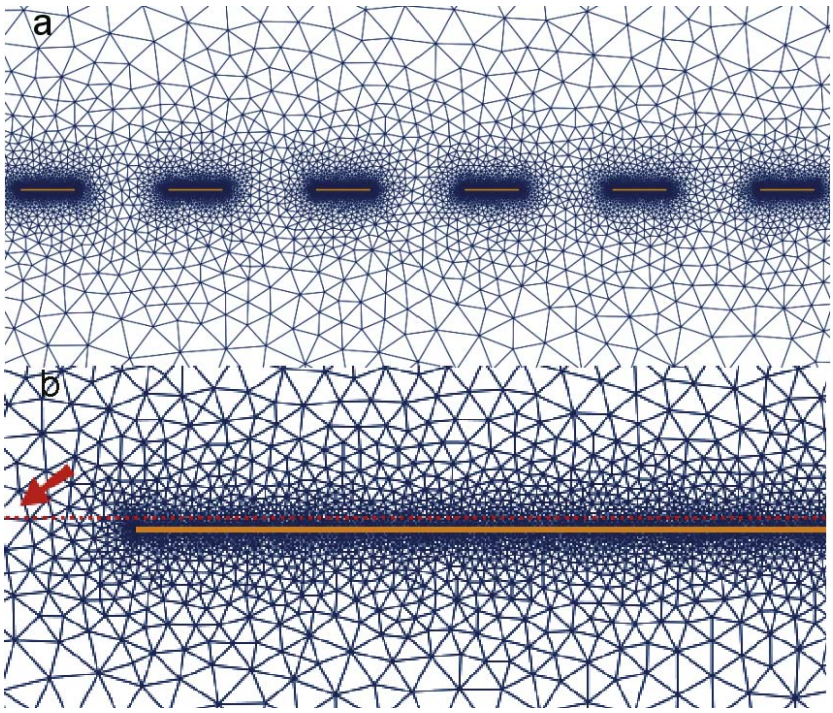


**Figure 2.** (a) Complete mesh and (b) detailed view near the edge of a superconducting filament. The red dashed line indicates the region of the simulated field profiles.

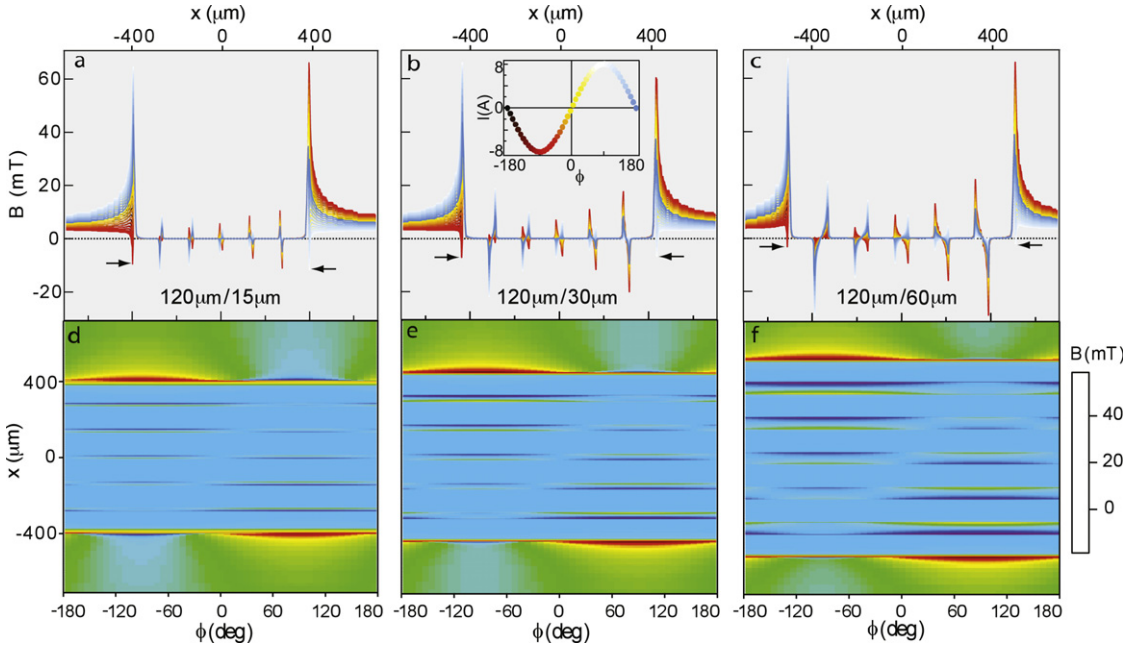


**Figure 3.** Magnetic field profiles at different phase points and corresponding time-dependent intensity maps for three multifilamentary geometries with filament/groove ratios corresponding to 8/1 (a) and (d), 4/1 (b) and (e), 2/1 (c) and (f). Phases and intensities of the applied current for the simulated magnetic profiles are shown in the inset of panel (b) using corresponding shades.

in figures 3(d)–(f) to present the time variations of the field more clearly. The magnetic flux partially penetrates into the filaments from the edges forming flux fronts. These as well as the flux free regions (Meissner state) in all the filaments remain constant during the cycle for all three different geometries (figures 3(a)–(c)). The flux profiles at the edges of the filaments alter during the cycle due to the self-field of the applied ac current. The magnetic flux distribution changes also for the three different geometries. Increasing the interfilament distance allows more flux to penetrate in the spacing between the filaments. Here, the peak intensity of the field profiles grows linearly with spacing (figures 3(b) and (c)). The flux

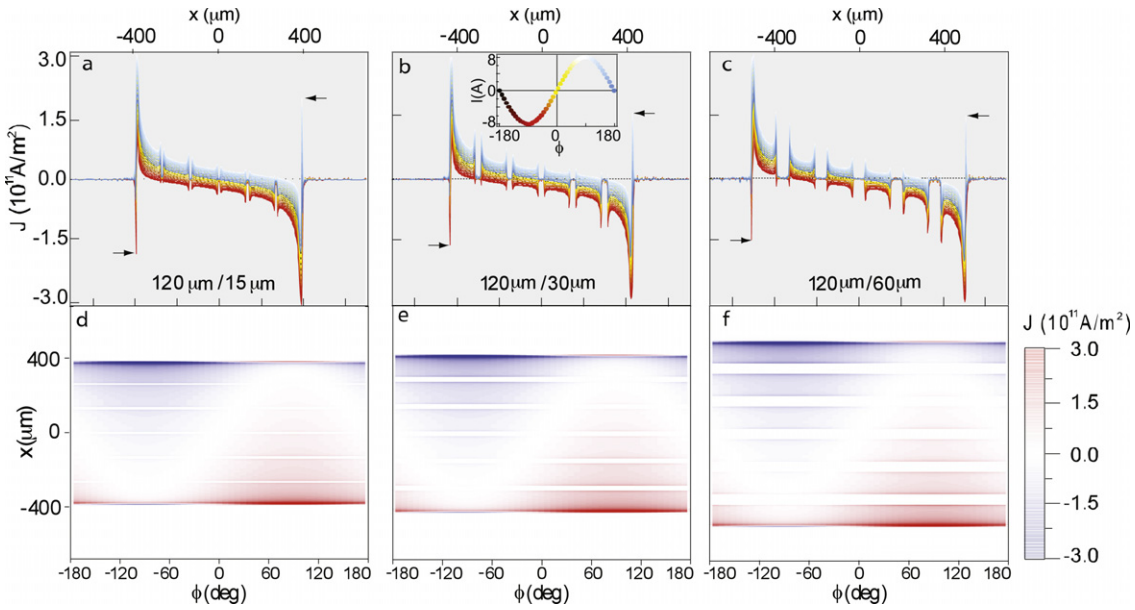


**Figure 4.** Current density profiles at different phase points and corresponding time-dependent intensity maps for three multifilamentary geometries with filament/groove ratios corresponding to 8/1 (a) and (d), 4/1 (b) and (e), 2/1 (c) and (f). Phases and intensities of the applied current for the simulated magnetic profiles are shown in the inset of panel (b) using corresponding colors.

profiles reach their maximum value of 65 mT at the edges of the two external filaments. The change in geometry does not affect the maximum value of the peaks in the flux profiles, but it alters the dips that form at the external edges of the sample, as indicated by black arrows in figures 3(a)–(c). This reveals a clear change in the way the sample screens the external magnetic flux for the different geometries. As the interfilament distance increases the coupling between the filaments is reduced and the screening behavior becomes more similar to independent filaments.

## 5. Current dynamics

The current dynamics provides additional useful information regarding the coupling between filaments. Figure 4 shows the current profiles at different phase points and the corresponding time-dependent current maps. The maps show at first glance how the current in each filament changes sign during each cycle, passing from positive (red) through zero (white) to negative (blue). Interestingly, a 'return current' of opposite sign (black arrows in figures 4(a)–(c)) flows in a narrow region at the edges of the left external filament in the first half cycle ($-180° < \phi < 0°$) and on the right external filament in the second half cycle ($-180° < \phi < 0°$). This current causes the steep variation from positive to negative flux observed in the same region of the field profiles (figure 3). A similar behavior has been observed in TRMOI measurements of single bridged YBCO thin films [17]. The return current is reduced by increasing the spacing between the filaments from 15 to 60 $\mu$m. The increased distance reduces the coupling between the filaments and redistributes the screening currents between the filaments. The growth of the peak intensity at the edges of all the filaments is further indication of the reduced coupling between the filaments. For the three different geometries the

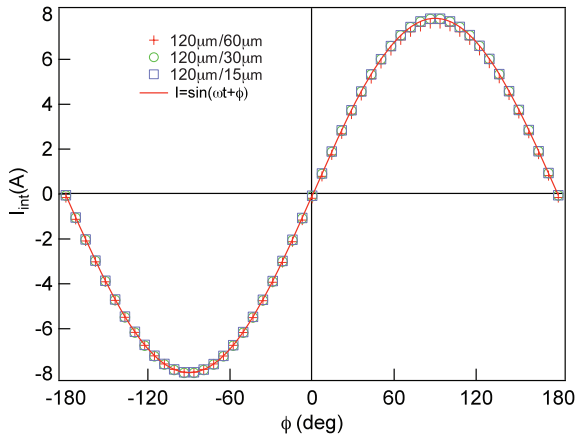


**Figure 5.** Total current flowing in all filaments calculated at different phase points for three different geometries, changing the filament width/groove ratio (symbols), and best fit (solid line).

current density in the two external filaments shows the most intense value corresponding to the critical current density $J_c = 3 \times 10^{11}$ A m$^{-2}$.

The current density profiles shown in figure 5 are obtained from the field profiles by inversion of the Biot–Savart law. This method has some limitations [18], but it allows direct comparison of the simulated results with experimental measurements [11]. The current profiles obtained by the inversion method differ only slightly from those calculated directly by the FE model. This procedure does not change the overall shape of the current profiles, neither does it affect their time-dependent behavior, but it smoothes and partially reduces the intensity of the peaks.

In figure 5 we show integrated current densities at different phase points and best fits for three simulated geometries. The

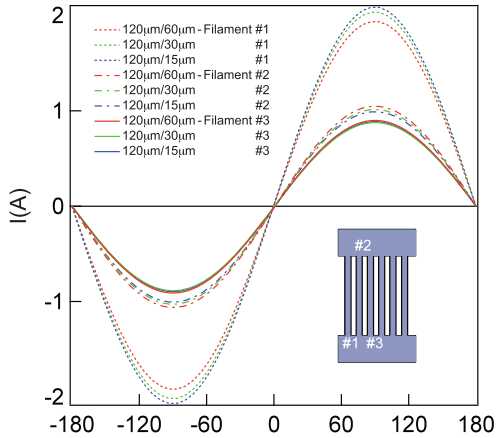


**Figure 6.** Transport current per filament in the first three filaments (inset) for three different geometries.

screening component of the current is symmetric, as shown by the field profiles (figure 3) and the current profiles (figure 4) at $\phi = -180°$, $0°$ and $180°$. Thus, the screening current is canceled out in the integration of the current density over all filaments and we obtain the transport current. Figure 5 shows that amplitude and phase of the transport current are not affected by the geometry. This quantitative analysis also confirms that the reduction of current intensity introduced by the inversion method is less than 1.3%.

Figure 6 shows the transport current per filament for three different geometries. Only the first three filaments are represented for clarity. The behavior of the other three filaments is completely symmetric. The current flows in each filament without any significant shift in phase with respect to the applied current. The current flows mostly in the external filaments for all geometries. The 120 $\mu$m/60 $\mu$m (120–60) geometry shows higher values of the current in the internal filaments as compared to the other geometries. As the distance between filaments is increased the transport current distributes more evenly.

## 6. Losses

The finite-element model is used to solve the PDE problem and to calculate the electric field. From current $J(t)$ and electric field $E(t)$ profiles, the instantaneous power losses can be calculated using the formula:

$$P(t) = |J(t) \cdot E(t)|. \tag{3}$$

Figure 7 shows the time-dependent losses for four different geometries with different filament width-spacing measured in $\mu$m: 120–15, 120–30, 120–60, and 120–90, respectively. The instantaneous losses decrease with increasing interfilament distance in the range $\phi = -36°$–$90°$, while in other regions the losses slightly increase. However, the values of the losses integrated over the whole cycle show an effective reduction of about 30% in the 120–90 geometry as compared to 120–15. Our model is presently being tested against experiments [16]. Once validated experimentally, it will be possible to use it to study low-loss geometries for manufacturing practical conductors. In particular, this type of analysis can be extended to YBCO coated conductors operating in HTS devices, such cables and coils, where the tapes are subjected to the electromagnetic interaction with neighbors. Such HTS applications, characterized by non-trivial geometries and a complex electromagnetic environment, are a typical example of situations that cannot be easily investigated with analytical models, and for which the finite-element approach is most useful.

## 7. Conclusions

We studied the field and current dynamics of a multifilamentary superconducting thin film by numerical simulation using a finite-element model to solve Maxwell's equations. We used a highly nonlinear resistivity to describe the electrical characteristics of the superconducting film. The model allows a direct comparison with measurements of local magnetic field variations performed by experimental techniques such as Hall probe scanning and arrays, SQUIDs, and TRMOI.

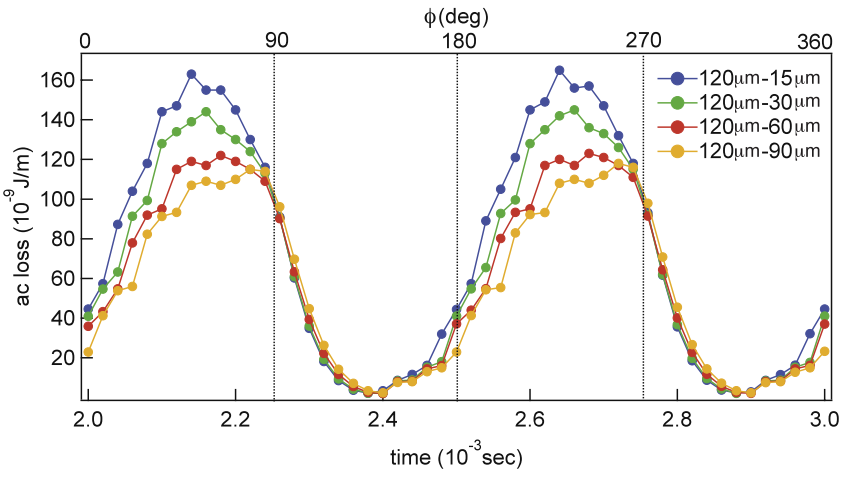


**Figure 7.** Instantaneous ac losses for four different geometries.

We observed that an increased interfilament distance alters the field and current dynamics due to reduced magnetic coupling between filaments. Screening and transport currents redistribute more evenly between all filaments which respond more independently. It also significantly reduces the losses of the multifilamentary thin films. Our model, once validated experimentally, can be used to study low-losses geometries for manufacturing practical conductors.

## Acknowledgments

This work was supported by the Mathematics of Information Technology and Complex System (MITACS) network. The work at CWM is supported by the DOE grant DEFG02-04ER46127.

## References

[1] Carr W J and Oberly C E 1999 *IEEE Trans. Appl. Supercond.* **9** 1475–8
[2] Ashworth S P and Grilli F 2006 *Supercond. Sci. Technol.* **19** 227–32
[3] Cobb C B, Barnes P N, Haugan T J, Tolliver J, Lee E, Sumption M, Collings E and Oberly C E 2002 *Physica* C **382** 52–6
[4] Majoros M, Glowacki B A, Campbell A M, Levin G A, Barnes P N and Polak M 2005 *IEEE Trans. Appl. Supercond.* **15** 2819–22
[5] Hazelton D W *et al* 2006 *AIP Conf. Proc.* **824** 859–68
[6] Duckworth R C *et al* 2007 *IEEE Trans. Appl. Supercond.* **17** 3159–62
[7] Sumption M D, Collings E W and Barnes P N 2005 *Supercond. Sci. Technol.* **18** 122–34
[8] Lucarelli A, Luepke G, Haugan T J, Levin G A and Barnes P N 2006 *Supercond. Sci. Technol.* **19** 667
[9] Dinner R B, Moler K A, Feldmann D M and Beasley M R 2007 *Phys. Rev.* B **75** 144503
[10] Ušák P, Polák M, Demenčík E, Kvitkovič J, Levin G A and Barnes P N 2007 *Supercond. Sci. Technol.* **20** 994–1001
[11] Lucarelli A *et al* 2007 *Appl. Phys.* A **88** 601–4
[12] Huebener R P 2001 *Magnetic Flux Structures in Superconductors* 2nd edn (Berlin: Springer) pp 245–51
[13] Paasi J and Lahtinen M 1998 *Physica* C **310** 57–61
[14] COMSOL Multiphysics http://www.comsol.com
[15] Brambilla R, Grilli F and Martini L 2007 *Supercond. Sci. Technol.* **20** 16–24
[16] Lucarelli A *et al* 2009 *J. Appl. Phys.* at press
[17] Lucarelli A *et al* 2008 *Supercond. Sci. Technol.* **21** 16–24
[18] Feldmann D M 2004 *Phys. Rev.* B **69** 144515